Aging and sperm signals alter DNA break formation and repair in the *C. elegans* germline

Erik Toraason[1¶], Victoria L. Adler[1¶], and Diana E. Libuda[1,*]

1 University of Oregon, Department of Biology, Institute of Molecular Biology, Eugene, OR, 97403

¶ These authors contributed equally to this work

* Corresponding Author (dlibuda@uoregon.edu)

Short title: DNA break formation and repair in aging oocytes

Abstract

Female reproductive aging is associated with decreased oocyte quality and fertility. The nematode *Caenorhabditis elegans* is a powerful system for understanding the biology of aging and exhibits age-related reproductive defects that are analogous to those observed in many mammals, including dysregulation of DNA repair. *C. elegans* germline function is influenced simultaneously by both reproductive aging and signals triggered by limited supplies of sperm, which are depleted over chronological time. To delineate the causes of DNA repair defects in aged *C. elegans* germlines, we assessed both DNA double strand break (DSB) induction and repair during meiotic prophase progression in aged germlines which were depleted of self-sperm, mated, or never exposed to sperm. We find that germline DSB induction is dramatically reduced only in hermaphrodites which have exhausted their endogenous sperm, suggesting that a signal due specifically to sperm depletion downregulates DSB formation. We also find that DSB repair is delayed in aged germlines regardless of whether hermaphrodites had either a reduction in sperm supply or an inability to endogenously produce sperm. These results demonstrate that in contrast to DSB induction, DSB repair defects are a feature of *C. elegans* reproductive aging independent of sperm presence. Finally, we demonstrate that the ubiquitin E2 ligase variant UEV-2 is required for efficient DSB repair specifically in young germlines, implicating UEV-2 in the regulation of DNA repair during reproductive aging. In summary, our study demonstrates that DNA repair defects are a feature of *C. elegans* reproductive aging and uncovers parallel mechanisms regulating efficient DSB formation in the germline.

Author Summary

Aging leads to a decline in the quality of the female reproductive cells, known as oocytes. Oocytes subjected to reproductive aging experience an increase in both infertility and aneuploidies that cause miscarriages and birth defects. The nematode *Caenorhabditis elegans* is a classic model system used to determine the mechanisms of aging. Old *C. elegans* oocytes accrue many defects which may contribute to their reduced quality, including dysregulation of DNA repair. *C. elegans* fertility and germline function is also regulated oocyte-independently by sperm-dependent signals. To determine how aging and sperm may independently impact DNA repair in aging *C. elegans* oocytes, we control oocyte aging and sperm presence independently to evaluate their effects on DNA break formation and repair. We find that running out of sperm reduces the levels of DNA breaks which are produced, but the efficiency of DNA repair declines during aging independent of sperm effects. We also identify a protein which specifically promotes DNA repair in the oocytes of young animals, suggesting that this protein may regulate DNA repair in the germline during aging. Taken together, our research defines aging-specific and aging-independent mechanisms which regulate the genome integrity of oocytes.

Introduction

Genome integrity must be preserved during gamete development, as any genetic defects incurred may have detrimental effects on progeny or fertility. Meiosis, the specialized cell division that generates haploid gametes such as eggs and sperm, utilizes specific DNA repair pathways to both ensure accurate chromosome segregation and preserve genomic integrity. During early meiotic prophase I, DNA double-strand breaks (DSBs) are intentionally induced across the genome by the conserved topoisomerase-like protein Spo11 (Keeney *et al.* 1997; Dernburg *et al.* 1998). A specific subset of these breaks must be repaired by recombination as crossovers, creating the physical connections between homologous chromosomes required for accurate chromosome segregation. Failure to repair meiotic DSBs accurately and efficiently can contribute to infertility or risk the formation of *de novo* germline mutations.

Gamete quality is negatively impacted in organisms of advanced chronological age (Broekmans *et al.* 2007). In many organisms, oocyte quality in particular declines starkly with maternal age (Luo *et al.* 2009, 2010; Moghadam *et al.* 2022). Oocyte aging is associated with conserved phenotypic changes, including loss of sister chromatid cohesion, dysregulation of DNA repair gene expression, and derepression of heterochromatin and retroviral elements (Luo *et al.* 2010; Achache *et al.* 2021; Raices *et al.* 2021; Chatzidaki *et al.* 2021; Wasserzug-Pash *et al.* 2022).

The nematode *Caenorhabditis elegans* is a key model system for the study of aging biology, including age-related infertility (Mack *et al.* 2018). *C. elegans* hermaphrodites (which produce oocytes as adults) undergo reproductive senescence due to declining oocyte quality and incur many of the defects observed in the aging mammalian ovary (Andux and Ellis 2008; Luo *et al.* 2009, 2010; Achache *et al.* 2021). Unlike many mammalian systems, however, which generate oocytes *in utero* and hold them in dictyate arrest until ovulation, *C. elegans*

hermaphrodites continuously produce new oocytes during their adult reproductive period (Albert Hubbard and Greenstein 2000). Mitotic proliferation and ovulation of oocytes is dependent upon signals from sperm, which are stored at the end of the germline in a specialized compartment called the 'spermatheca' (Mccarter *et al.* 1999; Cinquin *et al.* 2016). "Obligate female" mutants, which do not produce sperm, therefore exhibit dramatically slowed germline proliferation and progression (Doniach and Hodgkin 1984; Schedl and Kimble 1988; Mccarter *et al.* 1999; Cinquin *et al.* 2016). The *C. elegans* germline is organized in a spatial temporal gradient wherein oocytes mitotically proliferate at the distal tip and move proximally through the germline as they progress through meiotic prophase I (Albert Hubbard and Greenstein 2000).Thus, oocyte nuclei at all stages of meiotic prophase I are simultaneously present in the adult germline and enable assessment of meiotic events which are dynamic across prophase, such as the induction and repair of DSBs.

Multiple lines of evidence suggest that preservation of genome integrity is important for the maintenance of oocyte quality during reproductive aging. Human females carrying DNA repair protein variants exhibit extended fertility (Ruth *et al.* 2021). *C. elegans* mutants with extended reproductive periods are also resilient to exogenous DNA damage and upregulate genes associated with DNA repair (Luo *et al.* 2010). Further, recent evidence demonstrated that DNA damage and repair are altered in aged *C. elegans* germlines (Achache *et al.* 2021; Raices *et al.* 2021). By the fourth day of adulthood, *C. elegans* oocyte nuclei exhibit fewer programmed DSBs, delayed loading of recombination proteins, and increased engagement of error-prone repair mechanisms (Achache *et al.* 2021; Raices *et al.* 2021).

Sperm also regulate *C. elegans* germline physiology and reproduction. *C. elegans* hermaphrodites produce sperm only during a late stage in larval development (L'Hernault 2006). By the third to fourth day of adulthood, these sperm are depleted, which leads to a premature cessation of reproduction in *C. elegans* hermaphrodites (Luo *et al.* 2010). Sperm depletion also

induces broad transcriptional remodeling independent of aging processes, resulting in a 'female-like' transcriptional profile (Angeles-Albores *et al.* 2017). Mating extends the hermaphrodite reproductive span on average to the sixth day of adulthood, after which declining oocyte quality limits fertility (Luo *et al.* 2010). Mating and even exposure to males, however, also induces deleterious responses in hermaphrodites leading to premature demise (Maures *et al.* 2014; Shi and Murphy 2014). It remains unknown how reproductive aging, signaling induced by the presence or depletion of sperm, and mating intersect to regulate meiotic processes in aged *C. elegans* germlines.

To define DNA repair defects which are specific to reproductive aging, we assayed levels of DSB formation and repair in the meiotic oocytes of aged mated and unmated *C. elegans* hermaphrodites, as well as feminized germline mutants that do not produce sperm (*fog-2* mutants). We demonstrate that while the depletion of sperm downregulates DSB induction in aged germlines, delayed DSB repair is a shared feature of aging germlines independent of sperm presence. Finally, we identify the ubiquitin E2 ligase variant protein UEV-2 as a putative regulator of DNA repair during germline aging. Taken together, our work distinguishes DNA repair defects specific to reproductive aging and identifies parallel mechanisms regulating gamete quality in the immortal germline.

Methods

Caenorhabditis elegans strains and maintenance

Caenorhabditis elegans strains were maintained at 20°C on nematode growth medium (NGM) plates seeded with OP50 *Escherichia coli* bacteria. All experiments were performed in the N2 genetic background. Strains used in this experiment include AV761 (*GFP::cosa-1* II; *spo-11(me44)* IV/ nT1[qIs51]), AV676 (*GFP::cosa-1* II; *fog-2(q71)* V), N2 (wildtype), CB4108 (*fog-*

2(q71) V*)*, DLW135 (*uev-2(gk960600gk429008gk429009); rgr-1(gk429013)* III), DLW199 (libIs4[*pie-1p::uev-2::unc-54 3'UTR*] III:7007600), N2 (wild type), VC30168 (Million Mutation Project strain carrying *uev-2(gk960600)*), and WBM1119 (wbmIs60 [*pie-1p::3XFLAG::dpy-10 crRNA::unc-54* 3'UTR] (III:7007600)).

In experiments with aged animals, L4 hermaphrodites were isolated and maintained on NGM plates seeded with OP50 in the absence of males. Strains which produced self progeny were transferred to new NGM plates seeded with OP50 2 days post-L4 to prevent overconsumption of food from F1 progeny. At this transfer, if the experimental cohort was to be mated, young adult male N2 worms were additionally added to these plates at a ratio of ~1.5-2 males per hermaphrodite. Mated hermaphrodites were again transferred to new NGM plates with OP50 ~20-26 hours after males were added and male animals were discarded.

Strain DLW135 was generated by backcrossing VC30168 to N2 10 times. VC30168 was created by the Million Mutations Project (Thompson *et al.* 2013) and carried many mutations in addition to the *uev-2(gk960600)* allele of interest. Following backcrossing, mutations on Chromosomes I, II, IV, V, and X were assumed to have been eliminated. To determine the success of backcrossing on removing undesired mutations *in cis* with *uev-2* on Chromosome III, we assessed the presence of known flanking mutations to *uev-2(gk960600gk429008gk429009)*. Presence of the upstream most proximal genic mutation to *uev-2*, *pho-9(gk429005)*, was assessed via PCR amplification using OneTaq 2x Master Mix (forward primer DLO1142 5'-ACCCATTTCCCATTCAATCA-3' reverse primer DLO1143 5'-TTGTAATCTGCCCCAAAAGG-3') and subsequent HpaII restriction digest (New England Biolabs). DLW135 carried a wild type allele of *pho-9*, indicating that the region of Chromosome III upstream of *uev-2* was successfully reverted to wild-type sequence by recombination. However, the closely linked (~1 cM) downstream allele *rgr-1(gk429013)* was preserved in DLW135, as confirmed by Sanger sequencing (Sequetech) of a PCR amplified region of the *rgr-1* locus using OneTaq 2x Master

Mix (forward primer DLO1140 5'-TGGAATGGGACTTCCTCTTG-3' reverse primer DLO1141 5'-TTTCCAAAAGCCAGGACATC-3') isolated using a GeneJET PCR Purification kit (ThermoFisher). The *rgr-1(gk429013)* allele is a single base pair substitution resulting in a S360N missense mutation. RGR-1 is a Mediator complex subunit involved in transcriptional activation that is required for embryonic viability (Shim *et al.* 2002). S360N does not disrupt a predicted functional domain, and mutants carrying *rgr-1(gk429013)* survive embryogenesis and are fertile, indicating that this mutation does not severely disrupt function of the RGR-1 protein. As RGR-1 is not known to play a role in DNA damage repair, and *uev-2* has been previously demonstrated to modulate germline sensitivity to DNA damage (Luo *et al.* 2010), the phenotypes we observed using DLW135 in this manuscript are not best explained by the presence of the *rgr-1(gk429103)* mutation. For simplicity, DLW135 mutants are referred to as '*uev-2* mutants' in the text of this manuscript.

CRISPR/Cas9 genome editing

Strain DLW199 was generated using the SKILODGE transgenic system (Silva-García *et al.* 2019). WBM1119 was injected with 40ng/μL pRF4 purified plasmid, 40ng/μL purified PCR amplicon of the full *uev-2* coding sequence with 35bp homology arms to the wbmIs60 landing site (Phusion polymerase, forward primer DLO1144 5'-tcccaaacaattaaaaatcaaattttcttttccagATGCGAAGACGTAGCAACAG-3' reverse primer DLO1154 5'-taattggacttagaagtcagaggcacgggcgcgagatgTTAGTTTTCGATGTCAATTGGT-3'), 0.25 μg/μL Cas9 enzyme (IDT), 100ng/μL tracrRNA (IDT), and 56ng/μL crRNA DLR002 (5'-GCUACCAUAGGCACCACGAG-3'). Dpy F1 progeny were isolated and screened for insertion at the wbmIs60 locus by PCR following the SKILODGE recommended protocols (primers CGSG130, CGSG117 (Silva-García *et al.* 2019)).

The candidate insertion identified among progeny from the above injected hermaphrodites contained an undesired additional 43bp of sequence between the 5' 3xFLAG tag of the edited

wbmIs60 landing site and the start codon of the *uev-2* coding sequence. The strain carrying this insertion allele was backcrossed 3x to N2 and was CRISPR/Cas9 edited again to remove the undesired 5' sequence. Worms were injected with 0.25 μg/μL Cas9 (IDT), 100ng/μL tracrRNA (IDT), 28ng/μL gRNA DLR022 (5'-GAUCUUUAUAAUCACCGUCA-3'), 28ng/μL gRNA DLR023 (5'-UGUUGCUACGUCUUCGCAUC-3'), 25ng/μL ssODN donor DLO1173 (5'-AACAATTAAAAATCAAATTTTCTTTTCCAGATGCGGAGGCGAAGTAATAGACAATATGTTGATCTCTCATATTTTCGCGAAAC-3'), and 40ng/μL purified pRF4 plasmid. Successful removal of the 3xFLAG sequence and undesired 43bp inserted sequence were confirmed by PCR and Sanger sequencing (Sequetech).

Nematode irradiation

C. elegans worms were maintained at 20°C on NGM plates seeded with OP50 prior to and following irradiation. Irradiation was performed using a Cs^{137} source (University of Oregon).

Immunofluorescence sample preparation and microscopy

Immunofluorescence samples were prepared as in (Libuda *et al.* 2013). Nematodes were dissected in 1x Egg Buffer (118 mM NaCl, 48 mM KCl_2, 2 mM $CaCl_2$, 2 mM $MgCl_2$, 25 mM HEPES pH7.4, 0.1% Tween20) and were fixed in 1x Egg Buffer with 1% paraformaldehyde for 5 min on a SuperFrost Plus slide (VWR). Slides were then flash frozen in liquid nitrogen and the cover slip was removed before the slides were placed in ice cold methanol for 1 minute. Slides were washed in 1xPBST (1x PBS, 0.1% Tween20) 3x for 10 minutes before they were placed in Block (1xPBST with 0.7% bovine serum albumin) for a minimum of one hour. 50μL of primary antibody diluted in PBST (see below for specific antibody dilutions) was then placed on each slide and samples were incubated for 16-18hrs in a dark humidifying chamber with parafilm coverslips. Slides were then washed 3x in 1xPBST for 10 minutes. 50μL of secondary antibody diluted 1:200 in PBST were then added to each sample and slides were incubated for 2hr in a

dark humidifying chamber with parafilm coverslips. Slides were washed 3x in 1xPBST for 10 minutes, and then 50μL of 2μg/mL DAPI was applied to each slide. Samples were incubated in a dark humidifying chamber with parafilm coverslips for 5 minutes, then were washed 1x in PBST for 5 minutes. Slides were mounted with a No 1.5 coverslip (VWR) and sealed with nail polish. All slides were maintained at 4°C until imaging.

Immunofluorescence images were acquired at 512x512 or 1024x1024 pixel dimensions on an Applied Precision DeltaVision microscope with a 63x lens and a 1.5x optivar. All images were acquired in 3 dimensions with Z-stacks at 0.2μm intervals. In a minority of aged unirradiated germlines, we noted that most nuclei in mid-late pachytene exhibited high levels of RAD-51 and condensed DNA morphology characteristic of apoptosis. These aberrant gonads were not included in our analyses. Images were deconvolved with Applied Precision softWoRx software and individual image tiles were stitched into a single image for analysis using the Grid/Collection Stitching module in Fiji with regression threshold 0.7 (Preibisch *et al.* 2009) or using Imaris Stitcher software (Bitplane).

Specific antibodies used and their dilution factors are: Rabbit αRAD-51 (1:500), Chicken αRAD-51 (1:1000), Rabbit αDSB-2 (1:5000) (Rosu *et al.* 2013), Rabbit αGFP (1:1500), Chicken αGFP(1:1000), Alexa Fluor 488 Goat αChicken (1:200), Alexa Fluor 555 Goat αChicken (1:200), Alexa Fluor 555 Goat αRabbit (1:200), and Alexa Fluor 488 Goat αRabbit (1:200).

Image analysis and quantification

Images were analyzed as described in (Toraason *et al.* 2021). Image quantification was performed using Imaris software (Bitplane). Individual nuclei within stitched gonads were identified as Surface objects (Smooth 0.1-0.15, Background 3-4, Seed Point Diameter 3-4) based on DAPI staining intensity. Manual thresholding of specific values were used per gonad to generate surfaces which represented the nuclei observed. Defined surfaces were then split to

designate individual nuclei using the Imaris Surfaces Split module. Nuclei which were partially imaged or overlapped with other nuclei were eliminated from the analysis. RAD-51 foci were defined as Spot objects (Estimated XY Diameter 0.1, Model PSF-elongation 1.37, Background Subtraction enabled). To determine the number of RAD-51 foci per nucleus, we either utilized the "Find Spots Close to Surface" MATLAB module (Threshold value 0.1) or utilized the "Closest Distance to Surface" statistic calculated by Imaris to find the number of Spots ≤0.1μm distant from nuclei. The length of each germline was defined using the Imaris Measurements tool. Measurement points were specifically placed at the beginning of the premeiotic tip and the end of pachytene. For germlines which had a defined transition zone by DAPI morphology, points were also placed at the start and end of the transition zone.

Nuclei positions were transformed from 3D coordinates to a linear order using the Gonad Linearization Algorithm implemented in R (Toraason *et al.* 2021). Gonad length in germlines which lacked a defined transition zone (e.g. *fog-2* mutants, Supplemental Figure 2) was normalized to the distance from the premeiotic tip to the end of pachytene, where the premeiotic tip begins at position 0 and the end of pachytene is at position 1. In all other germlines, the gonad length was normalized to pachytene, where the beginning of pachytene is position 0 and the end of pachytene is position 1.

Germline DSB-2 staining was analyzed in Imaris using germlines stitched in Fiji as described above. The length of the germline was defined using the Imaris Measurements tool. Specific points were placed at the beginning of the transition zone, end of the transition zone, beginning of the DSB-2 zone (defined as the row of nuclei in which most nuclei had DSB-2 staining), the end of the DSB-2 zone, the final position of one or more nuclei which had DSB-2 staining, and the end of pachytene. The measured distances were then normalized to pachytene, where the beginning of pachytene is position 0 and the end of pachytene is position 1.

GFP::COSA-1 foci were quantified manually from late pachytene nuclei from 3D z-stacks using Fiji. Nuclei that were completely contained within the image stack were quantified in the last few rows of the late pachytene region in which all nuclei displayed bright GFP::COSA-1 foci (last ~3-6 rows of late pachytene in old *fog-2* germlines, last ~6-8 rows of late pachytene in young *fog-2* germlines).

***fog-2* Brood Viability Assay**

C. elegans worms were maintained at 20°C during fertility assays. Feminized *fog-2* mutants were synchronized in age by placing gravid mated CB4108 females onto an NGM plate seeded with OP50 for one hour. Hatched female progeny were isolated as L4s from these plates and were kept in isolation from males to prevent mating. At adult day 1, 2, 3, 4, or 5, these isolated *fog-2* females were then placed on individual plates with n=2 young adult N2 males each. Mated *fog-2* females were then subsequently transferred to new NGM plates seeded with OP50 with young adult N2 males at either 6hr, 12hr, 18hr, 24hr, and 48hr after the first mating, or at 24hr and 48hr after the first mating. 72hr after the first mating, adult females were discarded. Plates were scored ~24hr after the parent female was removed for hatched progeny, dead eggs, and unfertilized oocytes. Brood viability was calculated as (hatched progeny) / (hatched progeny + dead eggs). Fertility assays were replicated twice with n=5 females of each age group assayed per replicate.

During the course of the brood viability assays, some mated *fog-2* females exhibited matricidal hatching. This phenotype was more pronounced in aged worms, consistent with previous work which showed that matricidal hatching is exacerbated with maternal age (Pickett and Kornfeld 2013). Only eggs which were successfully ovulated were scored in the assay.

Statistics

All statistics were calculated in R (v4.0.3). Data wrangling was performed using the Tidyverse package (v1.3.0) (Wickham *et al.* 2019). Specific statistical tests used are denoted in the figure legends and text. P values were adjusted for multiple comparisons when appropriate. If 3 pairwise comparisons were being performed, Bonferroni correction was applied. If >3 pairwise comparisons were performed, Holm-Bonferroni correction was instead applied to reduce the risk of type II statistical errors.

Data and Code Availability

The gonad linearization algorithm is available on the Libuda Lab GitHub <github.com/libudalab/Gonad-Analysis-Pipeline> and on the Libuda Lab website <libudalab.org>

Results

Meiotic DNA break levels are influenced by both aging and sperm depletion

To determine the relative contributions of reproductive aging and sperm depletion to DNA break repair dynamics in the *C. elegans* germline, we examined DNA break levels in the oocytes of aged hermaphrodites which were mated (to prevent sperm depletion) or unmated (to permit sperm depletion) (Figure 1A). DNA breaks were quantified using immunofluorescence to visualize the recombinase RAD-51, which marks DSBs designated for repair by recombination (Gartner and Engebrecht 2022). While the cytological appearance of RAD-51 foci indicates the occurrence of DSBs, disappearance of RAD-51 foci indicates progression of a DSB event further through a DSB repair pathway. “Young” germlines were isolated from N2 hermaphrodites on the first day of adulthood (1 day post-L4, Figure 1A), while “aged” germlines were isolated from N2 hermaphrodites on their fourth day of adulthood (4 days post-L4, Figure 1A). Aged

hermaphrodites were maintained either unmated to males, or mated with males from their second to third day post-L4 larval stage (Figure 1A, see Methods).

To quantify the profile of DSB induction and repair across prophase I, we counted the number of RAD-51 foci per nucleus in oocytes from young and aged animals throughout the germline (see Methods). Under normal conditions, RAD-51 foci accumulate within nuclei following DSB induction by the conserved endonuclease SPO-11 in early pachytene (Dernburg *et al.* 1998; Colaiácovo *et al.* 2003). Then, as nuclei progress through mid and late pachytene, these RAD-51 foci decline in number as DSBs are repaired (Colaiácovo *et al.* 2003). During early pachytene, the amount of RAD-51 foci per nucleus was similar between aged mated germlines and young germlines (Figure 1B-C, Bin 2 Mann-Whitney U test $p=0.258$). Young germlines, however, accumulated a higher total number of RAD-51 foci per nucleus (Figure 1B-C, Bin 3 Mann-Whitney U test $p=0.005$), suggesting that DSB induction or RAD-51 loading is slightly compromised in aged mated germlines. We further noted that RAD-51 foci in aged unmated germlines were greatly decreased throughout early pachytene as compared to both young and aged mated germlines (Figure 1B-C, Bins 2-3 Mann-Whitney U test $p<0.001$), indicating that sperm depletion in aged germlines may affect meiotic DSB induction and/or RAD-51 loading.

In contrast to early pachytene, nuclei throughout mid pachytene from aged mated germlines maintained higher levels of RAD-51 than young germlines (Figure 1B-C, Bins 4-5 Mann-Whitney U test $p<0.05$). We observed a similar effect in the aged unmated germlines, which also displayed elevated numbers of RAD-51 foci relative to young germlines throughout mid pachytene (Figure 1B-C, Bins 4-5 Mann-Whitney U test $p<0.001$). Thus, DSB repair at mid-pachytene may be delayed in aging germlines regardless of mating or sperm depletion. Notably, by late pachytene the number of RAD-51 foci per nucleus converged between young, aged mated, and aged unmated germlines (Figure 1B-C, Bin 6 Mann-Whitney U test $p>0.05$),

355 indicating that ultimately all DSBs can be repaired or minimally offload RAD-51 in aged
356 germlines. Taken together, our results suggest that parallel mechanisms may regulate DNA
357 break levels in aged *C. elegans* germlines: 1) depletion of sperm downregulates DSB induction
358 and/or RAD-51 loading; and, 2) reproductive aging delays RAD-51 foci unloading at mid
359 pachytene.

360 To determine if the persistent RAD-51 foci in aged mated and unmated germlines were
361 derived from the programmed meiotic DSBs, we also examined RAD-51 foci in *spo-11(me44)*
362 null mutants, which do not form meiotic DSBs (Supplemental Figure 1) (Colaiácovo *et al.* 2003).
363 We did not observe a notable increase in nuclei with RAD-51 foci in aged *spo-11* germlines,
364 indicating that the persistent RAD-51 foci present at mid pachytene in aged wildtype gonads are
365 likely derived from normal meiotic functions and processes, such as SPO-11 activity.

366 Nuclei which are competent for DSB induction in the *C. elegans* germline have their
367 chromatin marked with the protein DSB-2 (Rosu *et al.* 2013). To assess if the altered
368 accumulation of DSBs which we observed in aged unmated germlines coincided with a change
369 in competency for DSB induction, we quantified the extent of young and aged germlines in
370 which ≥50% of nuclei exhibited DSB-2 staining (the "DSB-2 zone", Supplemental Figure 2A-B).
371 DSB-2 accumulates on meiotic chromatin beginning in the transition zone (leptotene/zygotene)
372 and is offloaded from the majority of nuclei by mid pachytene (Rosu *et al.* 2013; Toraason *et al.*
373 2021). Mutants which incur errors in crossover formation, however, maintain DSB-2 on meiotic
374 chromatin later into pachytene (Rosu *et al.* 2013). While the length of the DSB-2 zone was only
375 subtly altered in aged mated germlines (Supplemental Figure 2B-C, Mann-Whitney U test
376 $p=0.027$), the DSB-2 zone persisted later into pachytene in aged unmated germlines relative to
377 young germlines (Supplemental Figure 2B-C, Mann-Whitney U test $p=0.008$). Thus, our data
378 indicate that the extent of DSB-2 marked pachytene nuclei is influenced both by aging and by
379 the absence of sperm.

Meiotic DNA breaks are elevated in aged feminized germlines

To uncouple the relationship between sperm depletion and reproductive aging in regulating DSB induction and repair, we examined RAD-51 levels in germlines which have never been impacted by sperm or mating. Hermaphrodites carrying the *fog-2(q71)* mutation do not produce sperm during larval development but proliferate a full adult complement of oocytes (Schedl and Kimble 1988), rendering them “obligate females.” Due to the absence of signaling from sperm in *fog-2* mutants, both germline stem cell proliferation and meiotic progression are halted, such that meiotic oocytes are held within the gonad (Mccarter *et al.* 1999; Cinquin *et al.* 2016). Nonetheless, feminized mutants undergo reproductive senescence and exhibit reduced oocyte quality with age (Supplemental Figure 3; (Andux and Ellis 2008; Luo *et al.* 2009))

We analyzed the levels of RAD-51 foci in oocyte nuclei from young (1 day post-L4), aged (4 days post-L4), and old (6 days post-L4) *fog-2* germlines (Figure 2A-B). During our experiments we noted that the cytologically distinctive transition zone, which demarcates meiotic entry and is composed of nuclei undergoing active chromosome movement to facilitate pairing, was dramatically reduced in aged *fog-2* germlines (Supplemental Figure 4). Previous work has shown that mitotic germ cell proliferation is reduced in feminized and sperm-depleted germlines (Cinquin *et al.* 2016). Thus, the absence of a transition zone in aged *fog-2* germlines may be the product of two parallel effects: 1) nuclei in the transition zone completing the pairing process and therefore exhibiting the classic “cage-like” morphology of paired chromosomes found in pachytene nuclei; and, 2) decreased proliferation also limiting the number of new nuclei which enter meiosis. This lack of the transition zone in aged *fog-2* germlines presented a challenge for staging meiotic nuclei to make comparisons between young and aged gonads. To quantify RAD-51 levels in *fog-2* germlines independent of meiotic stages, we normalized the germline length with position 0 at the premeiotic tip and position 1 at the end of pachytene and used a sliding window to assay RAD-51 foci within the germline (Figure 2D, see Methods)

(Toraason *et al.* 2021). To describe the RAD-51 profile of aging *fog-2* germlines, we calculated two metrics: 1) the "RAD-51 zone" indicating the extent of the germline which contained nuclei with RAD-51 foci; and, 2) the "peak RAD-51 window" indicating the maximum levels of RAD-51 within the germlines.

To assess whether the proportion of germline nuclei with RAD-51 foci was altered in aging *fog-2* germlines, we calculated the "RAD-51 zone" of each age group, which was defined as the germline distance extending from the most distal (near the premeiotic tip) to the most proximal (near the end of pachytene) windows in which at least 50% of nuclei had one or more RAD-51 foci (Figure 2B, 2D). We found that the RAD-51 zone extended more distally in the germline in aged and old *fog-2* animals as compared to young germlines (Figure 2B, 2D). This distal expansion of the RAD-51 zone can likely be explained by transition zone nuclei in young germlines completing the pairing process and entering pachytene as the germline ages. In contrast, the proximal end of the RAD-51 zone only subtly shifted distally in aged and old germlines (Figure 2B, 2D). This result indicates that later prophase I nuclei within aged *fog-2* germlines continue to either maintain or induce RAD-51 marked DSBs.

To determine if the number of RAD-51 marked DSBs in *fog-2* germline nuclei were altered with age, we identified the "peak RAD-51 windows" in each age group, defined as the window in which the mean RAD-51 foci per nucleus was highest (Figure 2C, 2D arrowheads). We noted that the position of the peak RAD-51 window moved distally in aged and old *fog-2* germlines (Figure 2D arrowheads), suggesting that the spatial regulation of DSB induction and repair may change as feminized germlines age. The number of RAD-51 foci per nucleus within the peak RAD-51 window was not significantly different in aged germlines as compared to young gonads (Figure 2C-D, Mann-Whitney U test p=1.000). Old germlines, however, exhibited a significant ~1.5 fold increase in RAD-51 foci per nucleus as compared to young and aged germlines within the peak RAD-51 window, indicating that *fog-2* mutant germ cells accumulate

RAD-51 foci during aging (Figure 2C-D, Mann-Whitney U test p <0.001). This result notably differs from aged unmated wildtype germlines, which exhibit reduced DSBs with age (Figure 1B-C) (Achache *et al.* 2021; Raices *et al.* 2021). Our data therefore support a model in which sperm depletion, rather than absence of sperm, downregulates meiotic DSB induction.

DSB repair is altered in aged feminized germlines

The accumulation of RAD-51 foci observed in aging *fog-2* germlines may be the product of: 1) increased induction of DSBs; 2) defects in DSB repair; or, 3) a combination of these effects. To assess the efficiency of DSB repair during *fog-2* germline aging, we exposed young (1 day post-L4) and aged (4 days post-L4) *fog-2* mutant females to 5000 Rads of ionizing radiation (Figure 3A, Supplemental Figure 5), inducing ~118 DSBs per nucleus throughout the germline (Yokoo *et al.* 2012). We then allowed the animals to age for 2 days to resolve this DNA damage before assessing germlines for persistent unrepaired DSBs as marked by RAD-51 foci (Figure 3A). As *fog-2* germlines accumulate DSBs during aging (Figure 2C-D), we established baseline levels of DNA damage based on comparing RAD-51 foci in animals of equivalent ages that were never exposed to radiation to the irradiated cohorts (Figure 3A). We noted considerable inter-nucleus variance in the RAD-51 foci, which persisted following irradiation in both young and aged germlines (Supplemental Figure 5). This effect was particularly prominent in the distal germlines of both groups (Supplemental Figure 5C-D), suggesting that a subpopulation of nuclei in the mitotic germline or early stages of meiosis are uniquely susceptible to exogenous DNA damage regardless of parental age.

To estimate the residual DSBs derived from irradiation which were not yet repaired two days post irradiation, we calculated the median number of RAD-51 foci in a sliding window across the germline (Figure 3B, see Methods) and subtracted the unirradiated median RAD-51 foci from the irradiated median RAD-51 foci in each window (Figure 3C). Both young and aged germlines maintain high levels of damage in the distal germline following irradiation (germline

position 0.0-0.5, Figure 3C, Supplemental Figure 5C). Nuclei in the proximal region of young irradiated germlines did not consistently maintain median DNA break levels higher than baseline; whereas aged irradiated germlines maintained a median elevation of ~6-10 RAD-51 foci per nucleus (germline position 0.5-1.0, Figure 3C). This result indicates that aged *fog-2* germlines exhibit DNA repair defects specifically in nuclei at later stages of meiotic prophase I. Taken together, our experiments in "feminized" germlines demonstrate that DNA repair efficiency is altered in aging germlines independent of any signals from sperm.

Defects in meiotic DSB repair may disrupt the formation of interhomolog crossovers (Gartner and Engebrecht 2022). To determine if crossover recombination is impeded in aged *fog-2* germlines, we quantified bright GFP::COSA-1 foci, which mark joint molecules designated to become crossovers at late pachytene (Yokoo *et al.* 2012). Under normal conditions, each of the six pairs of *C. elegans* homologous chromosomes form one crossover and therefore most nuclei exhibit only six COSA-1 foci (Yokoo *et al.* 2012). We observed that the number of COSA-1 foci in late pachytene nuclei of old *fog-2* gonads were altered relative to their young counterparts (Figure 4A, Chi square test p=0.033), with a subtle but significant increase specifically in the fraction of nuclei with 7 COSA-1 foci (Figure 4A, Fisher's Exact test p=0.038). Thus, our data suggests that DSB repair in old *fog-2* germlines may be altered in a manner which impacts the number of designated crossovers. Further, the late pachytene region of the germline with bright COSA-1 foci was reduced in old *fog-2* germlines (Figure 4B). This phenotype is reminiscent of synapsis deficient mutants, which form COSA-1 foci only in a very small region of late pachytene (Cahoon *et al.* 2019). Previous work has shown that aged unmated wildtype germlines incur defects in crossover formation which reduce the number of crossovers formed (Luo *et al.* 2010; Achache *et al.* 2021; Raices *et al.* 2021). Our results in *fog-2* mutants therefore demonstrate that these defects are not shared in aged feminized *C.*

elegans germlines, suggesting that sperm presence influences the germ cell capacity for crossover formation during reproductive aging.

UEV-2 is required for 'youthful' germline DSB repair

To identify proteins which may regulate DSB repair in the aging *C. elegans* germline, we looked to candidate genes upregulated in long-reproductive *sma-2* mutant oocytes, which exhibit DNA damage resilience in addition to delayed reproductive senescence (Luo *et al.* 2010). The *sma-2* DNA damage resilience phenotype requires upregulation of the ubiquitin E2 ligase variant UEV-2, suggesting that this protein may promote efficient germline DNA repair (Luo *et al.* 2010). UEV proteins lack a catalytic cysteine residue conserved in E2 ubiquitin ligases (Sancho *et al.* 1998) but have been shown to form heterodimeric complexes with other E2 ubiquitin ligases to influence their function, implying regulatory roles for this protein class (Vandemark *et al.* 2001; Wijk and Timmers 2010).

To assess the influence of UEV-2 on DSB repair during germline aging, we utilized a strain carrying the putative null allele *uev-2(gk960600)*, which ablates the translation initiation site and second exon boundary of the gene (Supplemental Figure 6; see Methods). With the *uev-2* mutant strain, we examined the number of RAD-51 foci in germline nuclei derived from young (1 day post-L4) or aged (4 days post-L4) animals (Figure 5A). Aged *uev-2* mutants were also mated to avoid the DSB induction defects associated with sperm depletion (Figure 5A). If UEV-2 functions to promote efficient DSB repair in young gonads but becomes dysregulated or loses function during aging, then we would expect *uev-2* mutants to exhibit defects in DSB repair in young germlines but minimal additional defects in aged germlines. Indeed, when we compared the levels of RAD-51 observed in young and aged mated wildtype and *uev-2* germlines, we observed DSB repair defects that did not accumulate with age. In early pachytene, young and aged *uev-2* mutants exhibited similar levels of RAD-51 to young wildtype germlines (Figure 5B-C, Bins 2-3 Mann-Whitney U test $p>0.05$), indicating that UEV-2 is not

required for meiotic DSB induction nor RAD-51 loading. In contrast, at mid pachytene, young *uev-2* mutant germlines maintained elevated RAD-51 foci relative to young wildtype germlines (Figure 5B-C, Bins 4-5 Mann-Whitney U test $p<0.05$). The specific levels of DSBs at mid pachytene in young *uev-2* mutants were also indistinguishable from aged wildtype germlines (Figure 5B-C, Bins 4-5 Mann-Whitney U test $p>0.05$). These results at mid pachytene indicate that DSB repair is delayed in young *uev-2* mutants to an extent which recapitulates the effect we observe during wildtype aging. Aged *uev-2* germline RAD-51 levels at mid pachytene were statistically indistinguishable from either young or aged mated wildtype germlines (Figure 5B-C, Bins 4-5 Mann-Whitney U test $p>0.05$), suggesting that the *uev-2* mutation does not grossly exacerbate DSB repair defects with age.

In late pachytene, the specific rates of DSB resolution diverged slightly between young and aged *uev-2* and wildtype germlines (Figure 5B-C, Bins 6-7 Mann-Whitney U test $p<0.05$), suggesting that UEV-2-independent and age-specific effects may contribute to DSB resolution at this meiotic stage. Taken together, our results indicate that loss of *uev-2* in young germlines is sufficient to phenocopy the mid-pachytene patterns of DSB repair observed in an aged wildtype context. This observation supports a model in which UEV-2 functions in young germlines specifically to promote efficient DSB repair.

Overexpression of *uev-2* alters RAD-51 foci levels in an aged oocytes

As loss of *uev-2* in young germlines appeared to “prematurely age” RAD-51 foci patterns, we hypothesized that overexpression of *uev-2* in aged germlines could ameliorate persistent RAD-51 foci at mid pachytene. To test this hypothesis, we used CRISPR/Cas9 genome editing to generate a germline-specific overexpression construct of *uev-2* driven by the *pie-1* promoter (*pie-1p::uev-2*, see Methods). We then assessed for the presence of DSBs as marked by RAD-51 in the germlines of young (1 day post-L4) or aged (4 days post-L4) mated

528 animals overexpressing UEV-2 and compared those levels to young and aged mated wildtype
529 germlines (Figure 6A).

530 At the beginning of early pachytene, both young and aged mated *pie-1p::uev-2* mutants
531 initially accumulated DSBs at levels similar to young and aged mated wildtype gonads (Figure
532 6B-C, Bin 2 Mann-Whitney U test $p>0.05$). However, aged mated *pie-1p::uev-2* mutants
533 accumulated fewer total DSBs than young wildtype, aged mated wildtype, and young *pie-*
534 *1p::uev-2* germlines (Figure 6B-C, Bin 3 Mann-Whitney U test $p<0.05$). At mid pachytene, young
535 *pie-1p::uev-2* germlines maintained elevated RAD-51 foci over young wildtype germlines,
536 suggesting that overexpression of *uev-2* deleteriously impacted DSB repair in this context
537 (Figure 6B-C, Bin 4-5 Mann Whitney U test $p\leq0.001$). This effect was not preserved in aged
538 mated *pie-1p::uev-2* germlines, which exhibited similar DSB levels as young wildtype germlines
539 at the beginning of mid pachytene and slightly elevated foci at the end of mid pachytene (Figure
540 6B-C, Mann-Whitney U test Bin 4 $p=0.156$ Bin 5 $p=0.023$).

541 Throughout late pachytene, young *pie-1p::uev-2* germlines maintained subtle but
542 significantly elevated DSBs relative to young and aged wildtype germlines (Figure 6B-C, Bin 6-7
543 Mann-Whitney U test $p<0.05$). Conversely, aged mated *pie-1p::uev-2* germlines maintained
544 significantly fewer RAD-51 foci throughout late pachytene than young wildtype or young *pie-*
545 *1p::uev-2* germlines (Figure 6B-C, Bin 6-7 Mann-Whitney U test $p<0.05$). Taken together, these
546 data suggest that UEV-2 is not the sole regulator of DSB repair efficiency during *C. elegans*
547 germline aging and appears to have age-dependent functions in regulating meiotic DSB
548 accumulation and repair.

549

550 **Discussion**

551 *C. elegans* germline function is impacted both by reproductive aging and sperm signals.
552 Our study demonstrates that aged *C. elegans* germlines exhibit delayed DSB repair in mid-
553 pachytene regardless of mated status, suggesting that deficiencies in germline DNA repair are a

554 product of reproductive aging. We further find that sperm depletion, but not absence of sperm,
555 reduces RAD-51 marked DSBs at early pachytene, suggesting that loss of signals from sperm
556 downregulate DSB induction. Taken together, our study supports a model in which signals due
557 to sperm depletion and reproductive aging operate in parallel to influence meiotic DSB induction
558 and repair (Figure 7).

559 **Sperm depletion and DSB induction**

560 Our data indicate that aged unmated germlines exhibit dramatically reduced RAD-51 foci
561 in early pachytene (Figure 7). Previous work has similarly reported that unmated
562 hermaphrodites induce fewer DSBs with age (Achache *et al.* 2021; Raices *et al.* 2021). We find,
563 however, that mating is sufficient to rescue RAD-51 foci accumulation at early pachytene in
564 aged germlines. This effect in mated hermaphrodites may be due to cues from sperm-specific
565 signals, seminal fluid components, or male pheromones, all of which impact hermaphrodite
566 physiology (Shi and Murphy 2014; Aprison *et al.* 2022). While our study cannot distinguish
567 between these male- and mating-dependent effects, it is notable that aged feminized *fog-2*
568 germlines, which have never been exposed to sperm or males, do not exhibit reduced RAD-51
569 marked DSBs during aging. Thus, we propose that DSB induction in aged germlines is primarily
570 repressed by signals caused specifically from sperm depletion rather than reproductive aging,
571 mating-induced signaling, or exposure to males. We further found that *spo-11(me44)* mutants
572 do not exhibit increased DSBs with age, suggesting that the DSBs observed in aged gonads
573 come from the endogenous meiotic machinery. This result contrasts with previous work done
574 using *spo-11(ok79)* mutants, which incur SPO-11 independent DSBs with age (Raices *et al.*
575 2021). Thus, our data raises the possibility that the specific nature of *spo-11* mutation or
576 background strain-specific effects influence the occurrence of exogenous DSBs in aged
577 germlines.

578 Why might sperm depleted hermaphrodites downregulate germline DSB induction?
579 Recent evidence has unveiled a potential transition in hermaphrodite gonad function following

sperm depletion (Kern *et al.* 2021). After all sperm have been utilized from the spermatheca, hermaphrodites continue to lay unfertilized oocytes and secrete a nutrient-rich yolk in what has been suggested to be a form of 'primitive lactation' (Kern *et al.* 2021). Thus, the reduction in DSBs induced in germ cells following sperm depletion may be a product of the hermaphrodite germline functionally changing from a reproductive organ to a system which produces food for offspring. Reduced DSB formation, then, may be indicative of the metabolic resources of the hermaphrodite being reallocated in favor of providing nutritional supplement for progeny.

Multiple mutants in *C. elegans* have been reported to exhibit age-dependent decline in meiotic DSB induction (Tang *et al.* 2010; Rosu *et al.* 2013). Our research raises the possibility that these proteins may mediate or respond to signals from sperm. Also, both reproductive aging and *C. elegans* yolk secretion are regulated by insulin/insulin-like growth factor signaling (Luo *et al.* 2010; Kern *et al.* 2021). How reproductive aging and sperm depletion signals are integrated through this pathway to enact distinct phenotypes that impact germline function remains unknown but opens an avenue for future investigation. In summary, we have illuminated a regulatory mechanism specifically associated with sperm depletion which downregulates DSB induction in the *C. elegans* germline.

DSB repair and *C. elegans* reproductive aging

Aged *C. elegans* germlines exhibit multiple DNA repair defects, including delays in recombination protein loading and increased engagement of error-prone repair mechanisms (Raices *et al.* 2021). Both RAD-51 loading and error prone pathway engagement are regulated by DSB end resection (Gartner and Engebrecht 2022), suggesting that differences in DSB repair during aging may be derived from defects at this DNA processing step. We demonstrate that the E2 ligase variant UEV-2 is required for 'youthful' patterns of RAD-51 foci resolution during mid pachytene, indicating that a loss of UEV-2 or an age-related change in its function may underly the DNA repair defects in aged germlines. However, overexpression of UEV-2 is not sufficient to rescue persistent RAD-51 foci at mid pachytene in aged germlines and instead

606 introduces DSB repair defects in young germlines. These results suggest that the specific
607 levels of *uev-2* expression or the co-expression of other proteins may be important for the
608 function of UEV-2 in DNA repair processes.

609 While the specific molecular functions of UEV-2 remain unknown, previous yeast two-
610 hybrid assays have evidenced that UEV-2 may interact with BRC-1, the *C. elegans* BRCA1
611 homolog (Gudgen *et al.* 2004). BRCA1 is an E3 ubiquitin ligase thought to regulate many DNA
612 repair steps, including DSB resection (Cruz-García *et al.* 2014). Recent studies have
613 demonstrated that BRC-1 is vital for preventing error prone repair in the *C. elegans* germline (Li
614 *et al.* 2020; Kamp *et al.* 2020). Given these results, we propose that UEV-2 may modulate BRC-
615 1 activity in the germline to regulate resection of DSBs and promote efficient recombination.
616 Under this model, overexpression of *uev-2* or loss of its function may cause hyper- or hypo-DSB
617 resection respectively, and thus have a deleterious impact on the efficiency of recombination.
618 Taken together, our work demonstrates that UEV-2 is involved in regulating efficient and
619 'youthful' meiotic DSB repair, thereby opening avenues to future work uncovering the specific
620 roles this protein plays in meiosis.
621

622 **Acknowledgements**

623 We thank the CGC (funded by National Institutes of Health (NIH) P40 OD010440) for strains.
624 We thank C. Cahoon, A. Naftaly, and N. Kurhanewicz for thoughtful comments on this
625 manuscript. This work was supported by the National Institutes of Health T32GM007413 and
626 Advancing Science in America (ARCS) Foundation Award to E.T., and National Institutes of
627 Health R00HD076165 and R35GM128890 to D.E.L. D.E.L. is also a recipient of a March of
628 Dimes Basil O'Connor Starter Scholar award and Searle Scholar Award.
629

630 **Competing Interests**

631 The authors declare no competing interests.

Figures

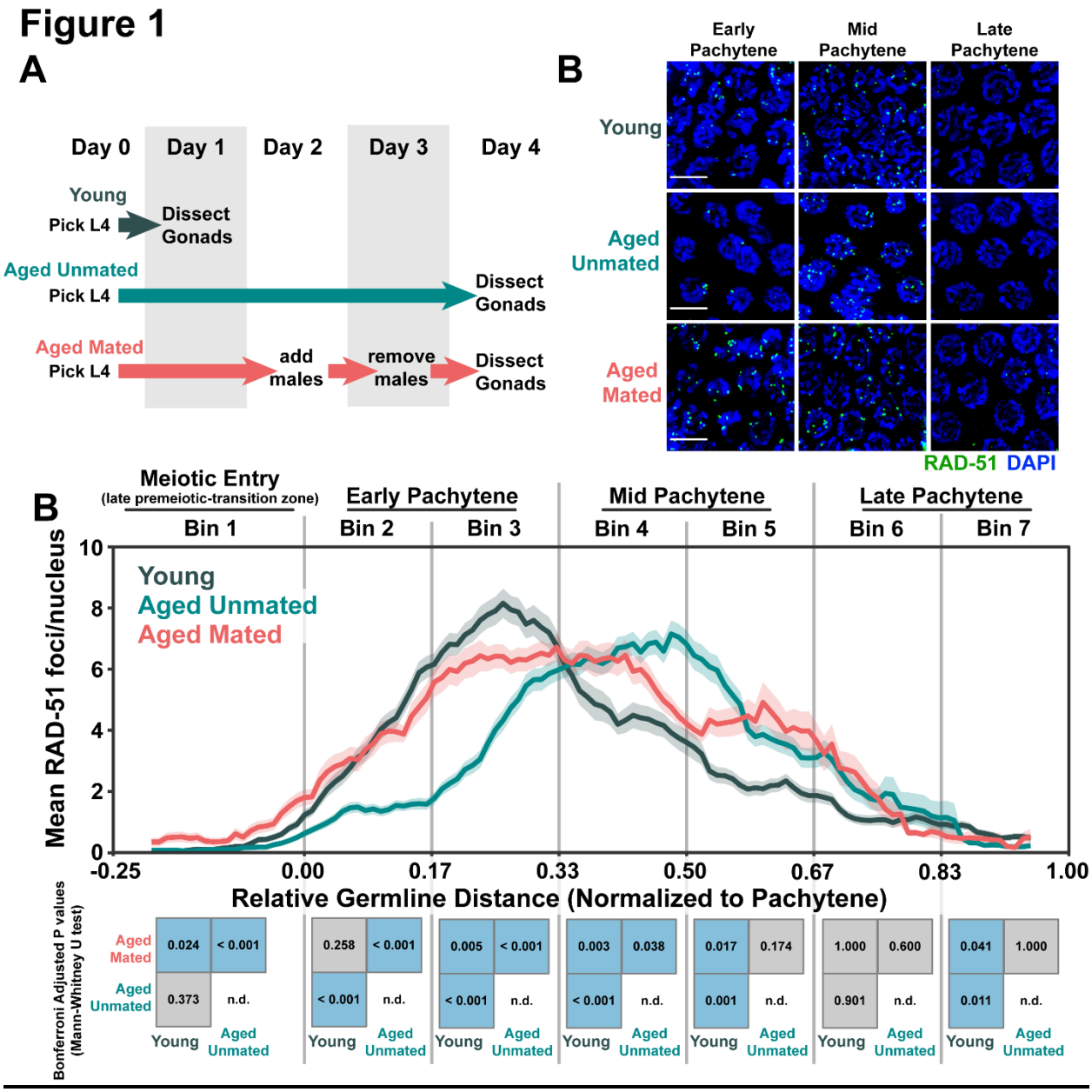

Figure 1. DNA double strand break levels are altered during *C. elegans* germline aging. A) Schemes used to isolate young (1 day post-L4) and aged (4 days post L4) worms for experiments. Days count ~18-24 hour periods after hermaphrodites were isolated as L4 larvae and are separated by alternating grey shaded boxes. B) Representative images of RAD-51 foci meiotic nuclei in young and aged germlines. Scale bars represent 5μm. C) RAD-51 foci per

nucleus in oocytes. Line plots represent the mean RAD-51 foci per nucleus along the length of the germline in a sliding window encompassing 0.1 units of normalized germline distance with a step size of 0.01 germline distance units. Mean RAD-51 foci were calculated from nuclei analyzed in n=9 total germlines derived from ≥3 experimental replicates within each age group. Shaded areas around each line represent ± SEM. Total nuclei analyzed (Bins 1/2/3/4/5/6/7) Young: 185/117/146/107/117/97/83; Aged Mated: 234/205/192/173/154/177/96; Aged Unmated: 268/147/161/175/191/152/110. Germlines distances were normalized to the start (0) and end (1) of pachytene based on DAPI morphology (see Methods). For analysis, the germline was divided into 7 bins encompassing the transition zone (Bin 1), early pachytene (Bins 2-3), mid pachytene (Bins 4-5), and late pachytene (Bins 6-7). The germline positions at which each bin start and end are marked on the X axis as vertical grey lines. Heat maps below each bin display the p values of pairwise comparisons of RAD-51 foci per nucleus counts within that bin. P values were calculated using Mann-Whitney U tests with Bonferroni correction for multiple comparisons. Blue tiles indicate significant differences (adjusted p value <0.05) and grey tiles indicate nonsignificant effects (adjusted p value >0.05).

Figure 2

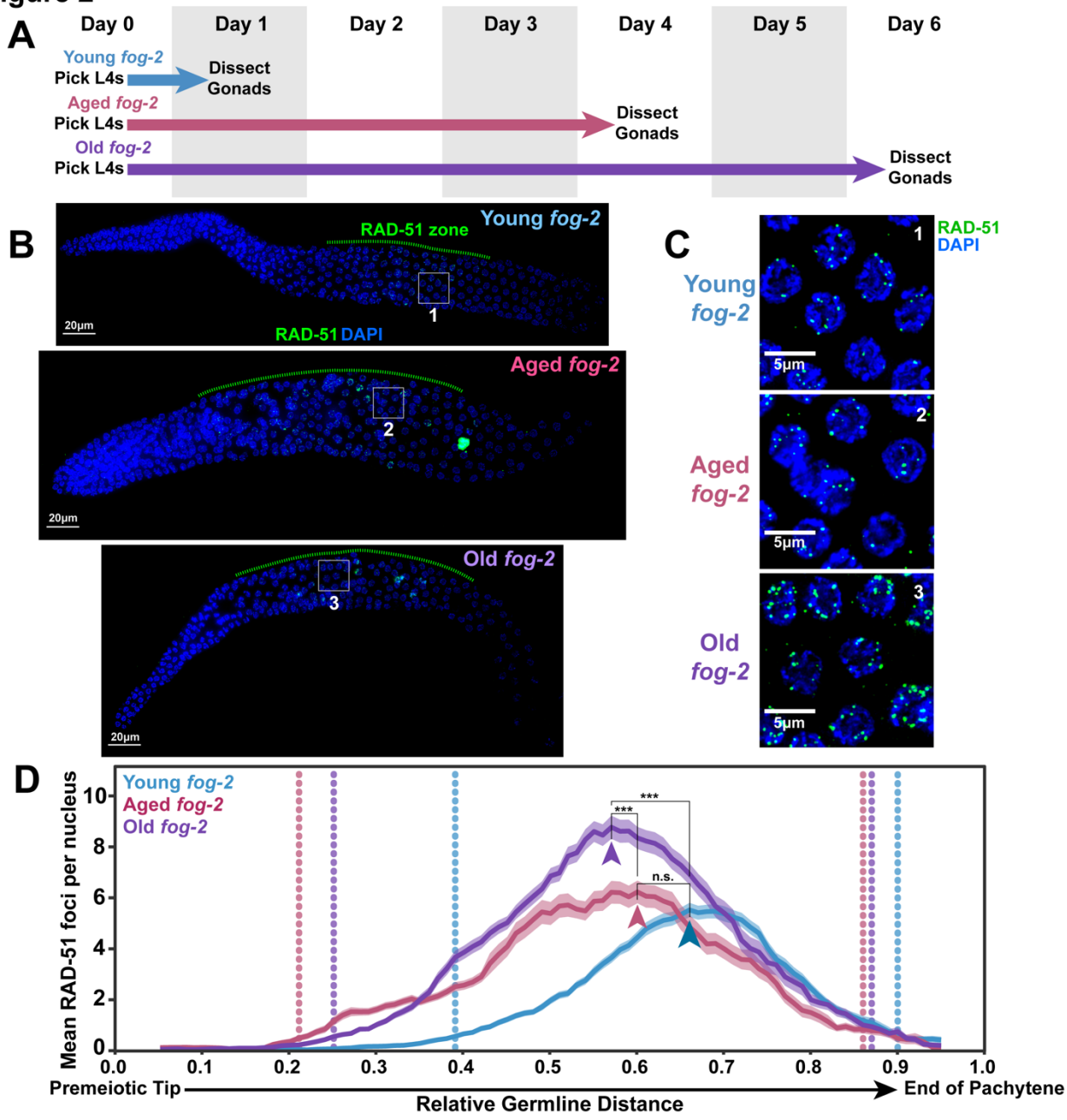

Figure 2. DNA double strand break levels increase with age in *fog-2* feminized germlines. A) Schemes used to isolate young (1 day post-L4), aged (4 days post L4), and old (6 days post L4) *fog-2(q71)* worms for experiments. Days count ~18-24 hour periods after hermaphrodites were isolated as L4 larvae and are separated by alternating grey shaded boxes. B) Representative whole germline images of young, aged, and old *fog-2* germlines. The RAD-51

zone, defined as the region of the germline in which the majority of nuclei have one or more RAD-51 foci, is indicated with a green dashed line. All germlines are oriented with the distal mitotic tip on the left and the end of pachytene on the right. Scale bars represent 20μm. Grey numbered boxes indicate the positions of the images presented in panel C. C) Representative images of the peak levels of RAD-51 foci observed in meiotic nuclei of young, aged, and old *fog-2* germlines. Scale bars represent 5μm. Each panel is numbered to indicate the position in the germlines displayed in panel B that each inset was taken from. D) RAD-51 foci per nucleus in *fog-2(q71)* oocytes. Line plots represents the mean RAD-51 foci per nucleus along the length of the germline in a sliding window encompassing 0.1 units of normalized germline distance with a step size of 0.01 germline distance units. Mean RAD-51 foci were calculated from nuclei analyzed in n=9 total germlines derived from ≥3 experimental replicates within each age group. Shaded areas around each line represent ± SEM. Average nuclei quantified in each bin ± standard deviation: Young *fog-2* 173±21.3, Aged *fog-2* 143±32.0, Old *fog-2* 148.5±29.6. Germline distance was normalized to the premeiotic tip (0) and end of pachytene (1) based on DAPI morphology (see Methods). Arrowheads indicate the “peak RAD-51” windows, defined as the windows along the length of the germline of each age group with the highest RAD-51 foci per nucleus. P values were calculated by Mann-Whitney U test comparisons of RAD-51 counts within these peak windows with Bonferroni correction for multiple comparisons (n.s. = $p>0.05$, *** = $p<0.001$). Vertical dotted lines indicate the distal and proximal bounds of the RAD-51 zone for each age group, defined as windows in which the median RAD-51 foci per nucleus count was ≥1.

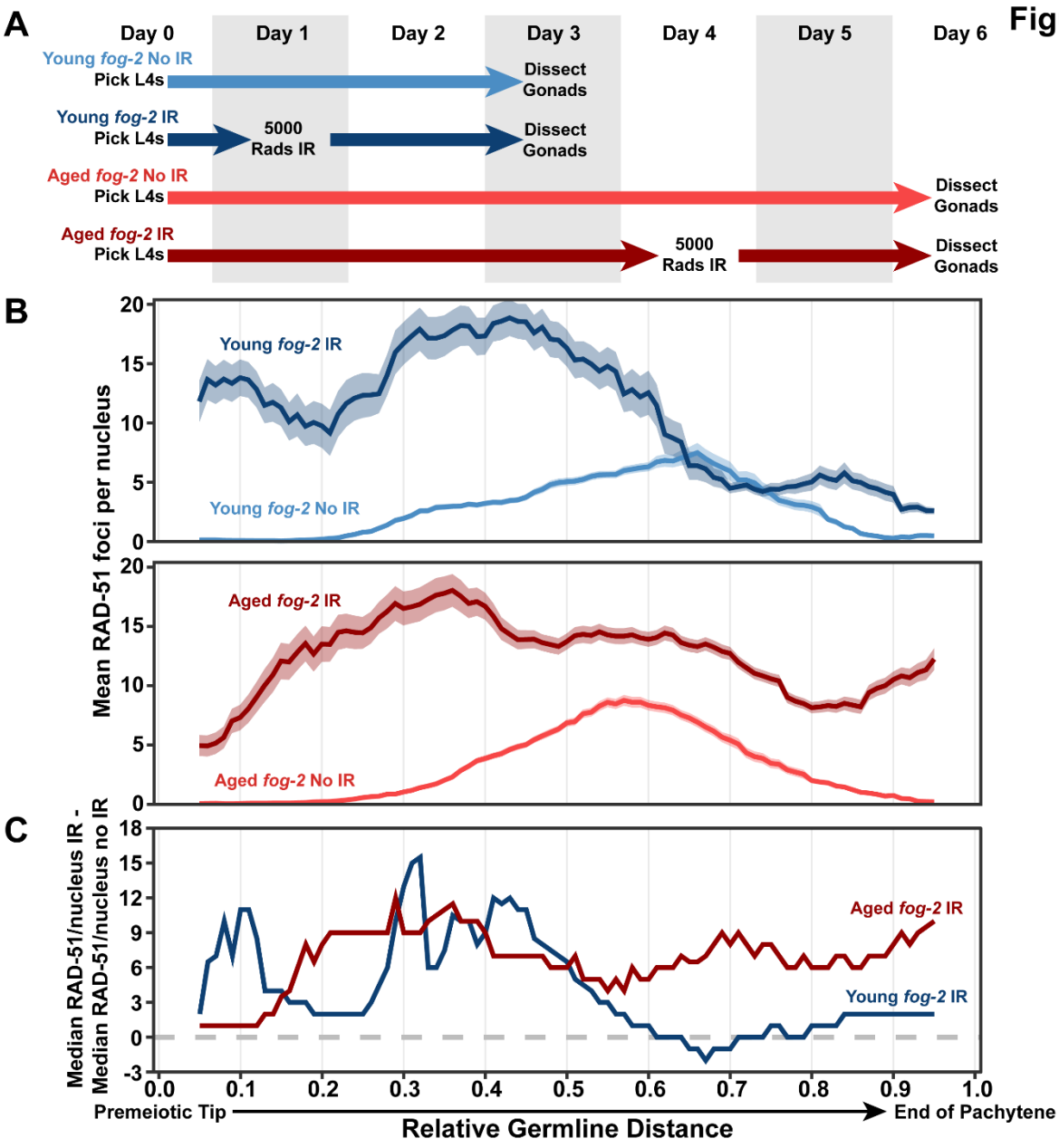

Figure 3. DNA double strand break repair is disrupted in aged *fog-2* feminized germlines. A) Schemes used to isolate young and aged *fog-2(q71)* worms for experiments. Days count ~18-24 hour periods after hermaphrodites were isolated as L4 larvae and are separated by alternating grey shaded boxes. Irradiated (IR) germlines were exposed to ionizing radiation at the first or fourth day of adulthood and were allowed to recover for two days before analysis (see Methods). Unirradiated germlines (No IR) were never exposed to radiation. B) RAD-51 foci

691 per nucleus in irradiated (IR) and unirradiated (no IR) oocytes. Line plots represents the mean
692 RAD-51 foci per nucleus along the length of the germline in a sliding window encompassing 0.1
693 units of normalized germline distance with a step size of 0.01 germline distance units. Plots in
694 panel B share an X axis with the plot in panel C. Mean RAD-51 foci were calculated from nuclei
695 analyzed in n=9 total germlines derived from ≥3 experimental replicates within each age group.
696 Shaded areas around each line represent ± SEM. Average nuclei quantified in each bin ±
697 standard deviation: Young *fog-2* No IR 141.6±26.6, Young *fog-2* IR 134.4±27.9, Old *fog-2* No IR
698 148.5±29.6, Old *fog-2* IR 142.4±30. Germline distance was normalized to the premeiotic tip (0)
699 and end of pachytene (1) based on DAPI morphology (see Methods). Representative images of
700 young and aged IR and No IR germlines are displayed in Supplemental Figure 5. C) Median
701 RAD-51 foci per nucleus in irradiated germlines above median levels in unirradiated germlines
702 of the same age (calculated as median RAD-51 foci in IR gonads – median RAD-51 foci in non-
703 IR gonads within each window along the length of the germline).
704

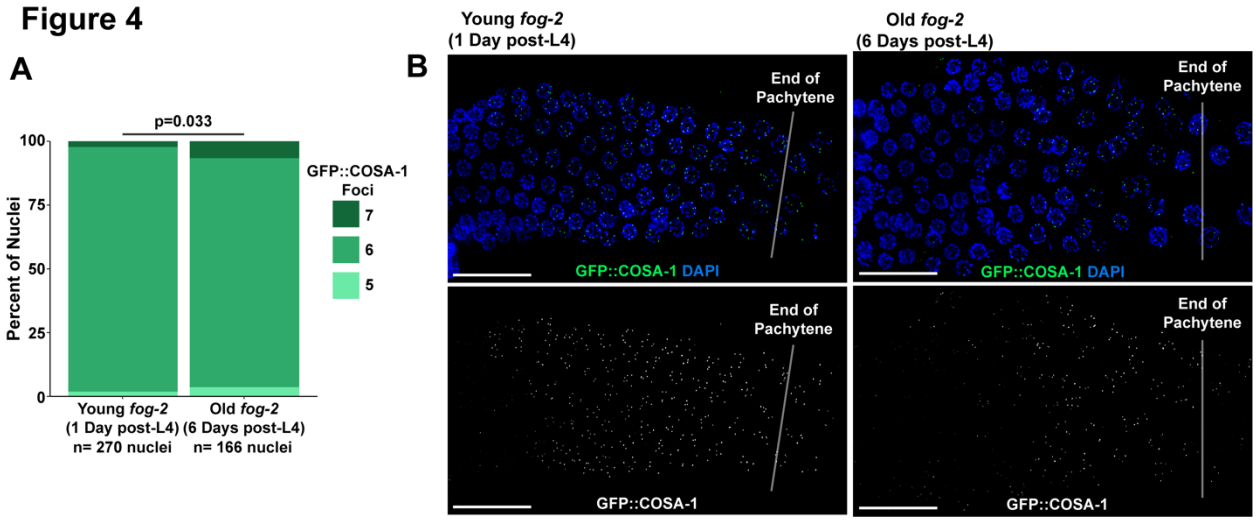

Figure 4. Crossover designation is altered in aged *fog-2* germlines. A) Stacked bar plot of the percent of nuclei in young (1 day post L4) and old (6 days post L4) *fog-2* mutants with the given number of GFP::COSA-1 foci. The p value displayed was calculated by Chi Square test. N values indicate the number of nuclei scored. B) Representative images of GFP::COSA-1 localization in young and old *fog-2* mutant germlines. Scale bars represent 20μm. Germlines are oriented with the proximal end on the left and distal end on the right. Vertical low opacity white lines designate the end of pachytene.

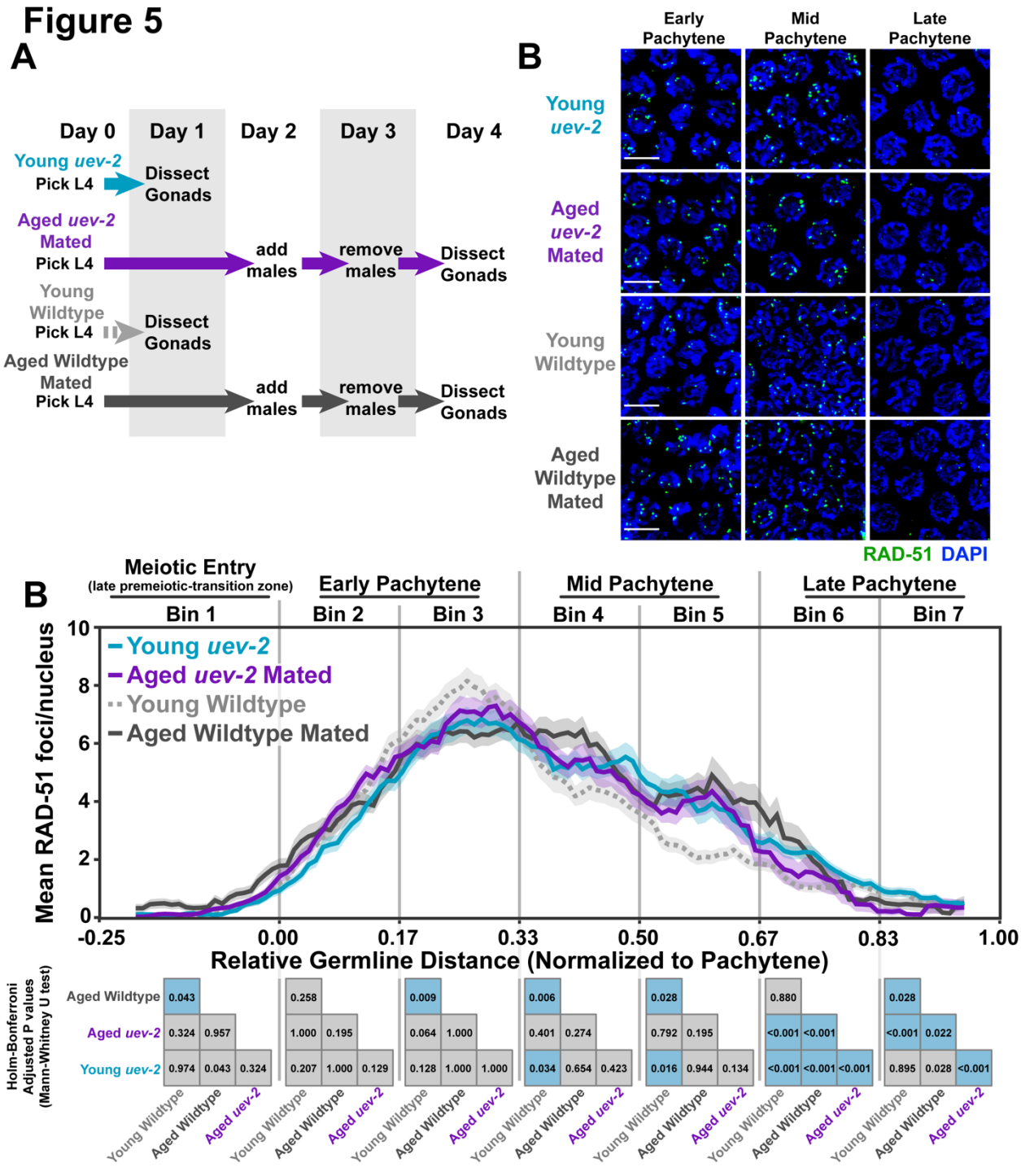

Figure 5. UEV-2 is required for 'youthful' DNA repair. A) Schemes used to isolate young (1 day post-L4) and aged (4 days post L4) *uev-2* mutant worms for experiments. Days count ~18-24 hour periods after hermaphrodites were isolated as L4 larvae and are separated by alternating grey shaded boxes. B) Representative images of RAD-51 foci in meiotic nuclei of

young *uev-2*, aged mated *uev-2*, young wildtype, and aged mated wildtype germlines. Scale bars represent 5μm. C) RAD-51 foci per nucleus in oocytes. Line plots represent the mean RAD-51 foci per nucleus along the length of the germline in a sliding window encompassing 0.1 units of normalized germline distance with a step size of 0.01 germline distance units. Mean RAD-51 foci were calculated from nuclei analyzed in n=9 total germlines derived from ≥3 experimental replicates within each age and genotype group. Shaded areas around each line represent ± SEM. Total nuclei analyzed (Bins 1/2/3/4/5/6/7) Young Wildtype: 185/117/146/107/117/97/83; Aged Wildtype Mated: 234/205/192/173/154/177/96; Young *uev-2*: 186/135/134/113/112/132/95; Aged *uev-2* Mated: 129/161/155/158/167/142/120. Germlines distances were normalized to the start (0) and end (1) of pachytene based on DAPI morphology (see Methods). For analysis, the germline was divided into 7 bins encompassing the transition zone (Bin 1), early pachytene (Bins 2-3), mid pachytene (Bins 4-5), and late pachytene (Bins 6-7). The germline positions at which each bin start and end are marked on the X axis as vertical grey lines. Heat maps below each bin display the p values of pairwise comparisons of RAD-51 foci per nucleus counts within that bin. P values were calculated using Mann-Whitney U tests with Holm-Bonferroni correction for multiple comparisons. Blue tiles indicate significant differences (adjusted p value <0.05) and grey tiles indicate nonsignificant effects (adjusted p value >0.05).

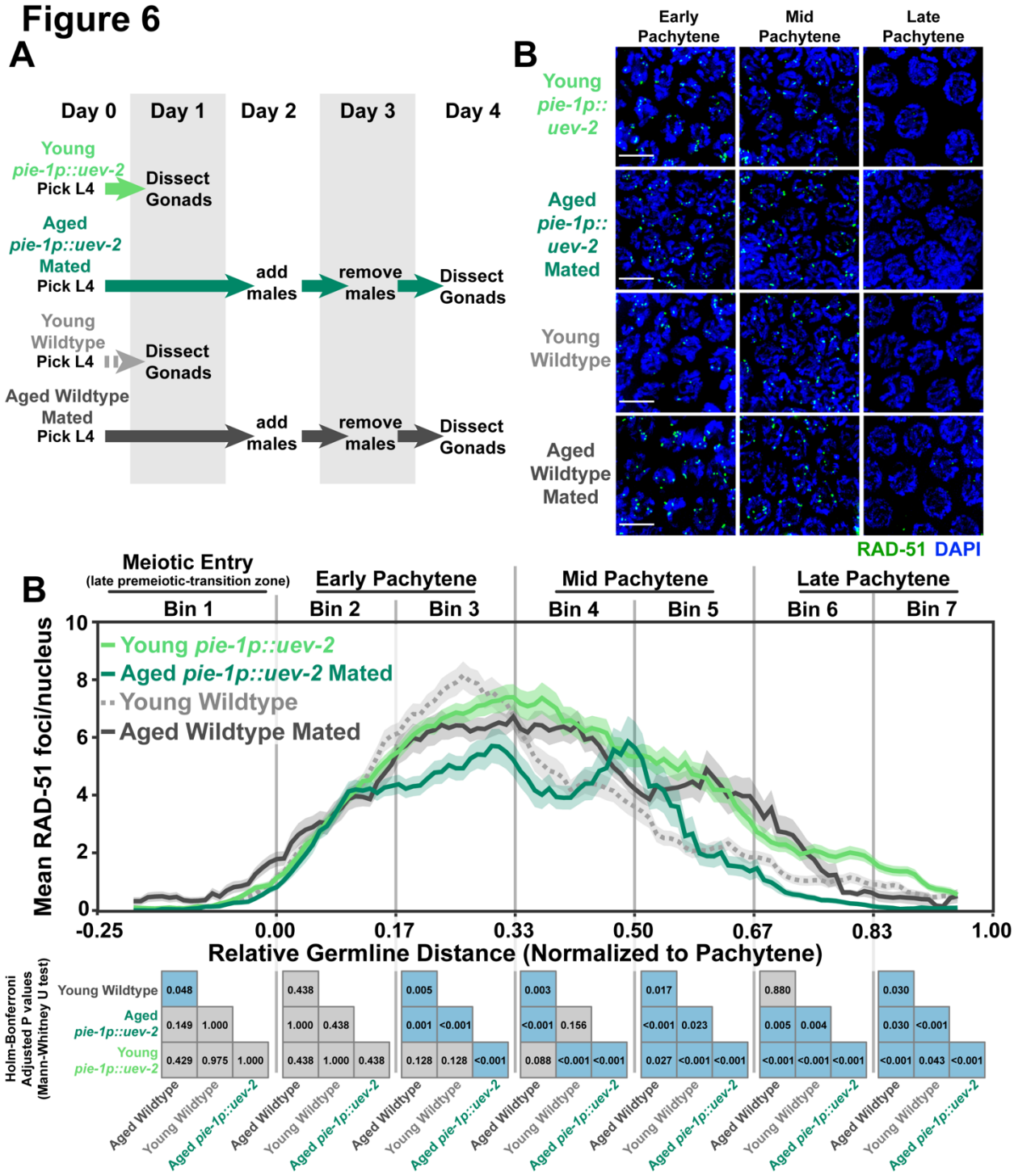

Figure 6. Germline *uev-2* overexpression differentially impacts DSB levels in young and aged germlines. A) Schemes used to isolate young (1 day post-L4) and aged (4 days post L4) worms for experiments. Days count ~18-24 hour periods after hermaphrodites were isolated as

L4 larvae and are separated by alternating grey shaded boxes. B) Representative images of RAD-51 foci in meiotic nuclei of young *pie-1p::uev-2*, aged *pie-1::uev-2*, and young wildtype germlines. Scale bars represent 5μm. C) RAD-51 foci per nucleus in oocytes. Line plots represent the mean RAD-51 foci per nucleus along the length of the germline in a sliding window encompassing 0.1 units of normalized germline distance with a step size of 0.01 germline distance units. Mean RAD-51 foci were calculated from nuclei analyzed in n=9 total germlines derived from ≥3 experimental replicates within each age group. Shaded areas around each line represent ± SEM. Total nuclei analyzed (Bins 1/2/3/4/5/6/7) Young Wildtype: 185/117/146/107/117/97/83; Aged Wildtype Mated: 234/205/192/173/154/177/96; Young *pie-1p::uev-2*: 182/192/162/125/116/97; Aged *pie-1p::uev-2* Mated: 140/149/136/127/126/95/102. Germlines distances were normalized to the start (0) and end (1) of pachytene based on DAPI morphology (see Methods). For analysis, the germline was divided into 7 bins encompassing the transition zone (Bin 1), early pachytene (Bins 2-3), mid pachytene (Bins 4-5), and late pachytene (Bins 6-7). The germline positions at which each bin start and end are marked on the X axis as vertical grey lines. Heat maps below each bin display the p values of pairwise comparisons of RAD-51 foci per nucleus counts within that bin. P values were calculated using Mann-Whitney U tests with Holm-Bonferroni correction for multiple comparisons. Blue tiles indicate significant differences (adjusted p value <0.05) and grey tiles indicate nonsignificant effects (adjusted p value >0.05).

Figure 7

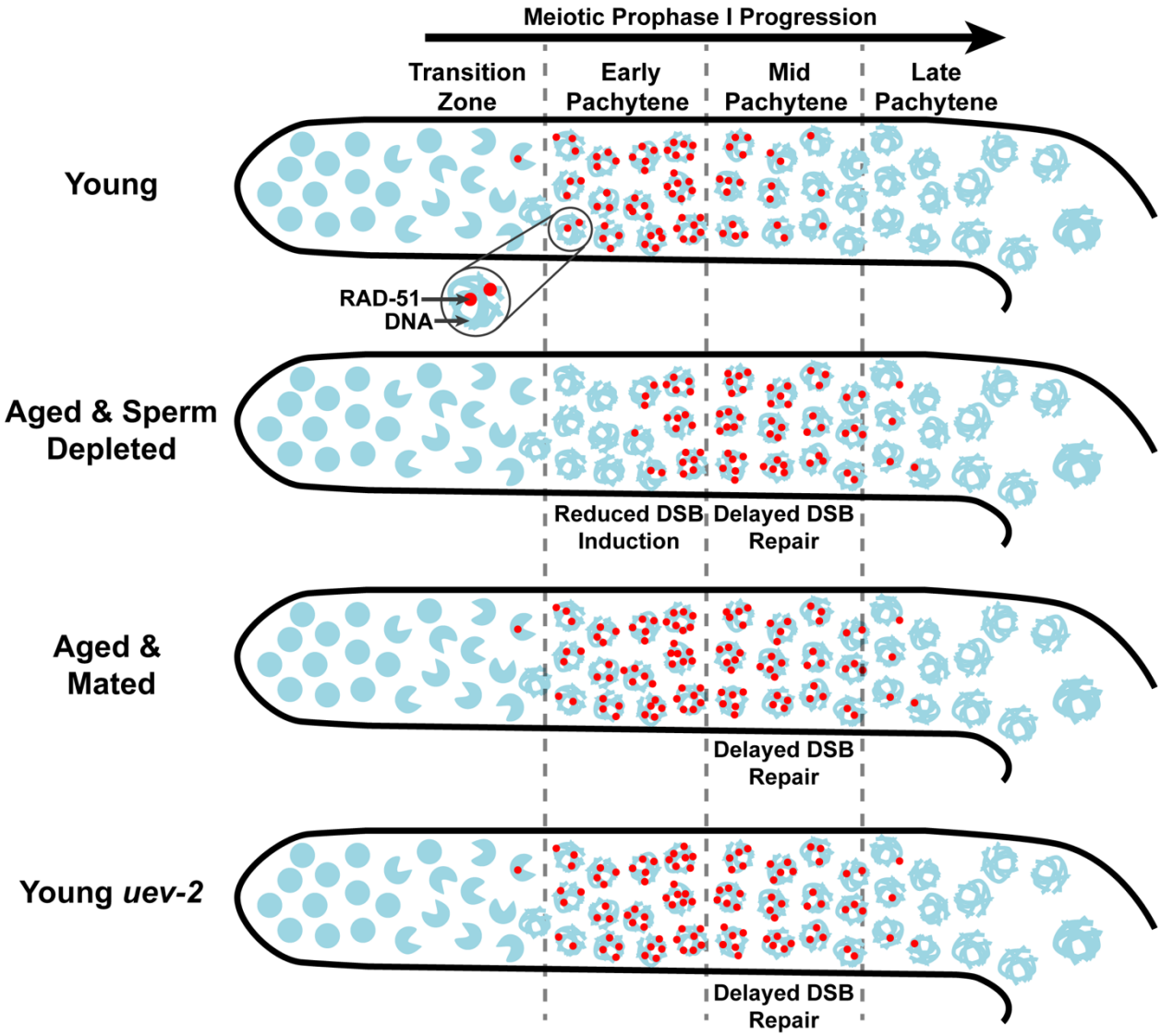

762

763 **Figure 7. Model of aging and sperm effects on DSB levels during germline aging.**

References

Achache H., R. Falk, N. Lerner, T. Beatus, and Y. B. Tzur, 2021 Oocyte aging is controlled by mitogen-activated protein kinase signaling. Aging Cell 20.

Albert Hubbard E. J., and D. Greenstein, 2000 The Caenorhabditis elegans gonad: A test tube for cell and developmental biology. Dev. Dyn. 218: 2–22.

Andux S., and R. E. Ellis, 2008 Apoptosis maintains oocyte quality in aging Caenorhabditis elegans females. PLoS Genet. 4.

Angeles-Albores D., D. H. W. Leighton, T. Tsou, T. H. Khaw, I. Antoshechkin, *et al.*, 2017 The Caenorhabditis elegans female-like state: Decoupling the transcriptomic effects of aging and sperm status. G3 Genes, Genomes, Genet. 7: 2969–2977.

Aprison E. Z., S. Dzitoyeva, and I. Ruvinsky, 2022 Serotonin coordinates reproductive functions in Caenorhabditis. BioRXiv.

Broekmans F. J., E. A. H. Knauff, E. R. te Velde, N. S. Macklon, and B. C. Fauser, 2007 Female reproductive ageing: current knowledge and future trends. Trends Endocrinol. Metab. 18: 58–65.

Cahoon C. K., J. M. Helm, and D. E. Libuda, 2019 Synaptonemal Complex Central Region Proteins Promote Localization of Pro-crossover Factors to Recombination Events During Caenorhabditis elegans Meiosis. Genetics 213: 395–409.

Chatzidaki E. E., S. Powell, B. J. H. Dequeker, J. Gassler, M. C. C. Silva, *et al.*, 2021 Ovulation suppression protects against chromosomal abnormalities in mouse eggs at advanced maternal age. Curr. Biol. 31: 4038-4051.e7.

Cinquin A., M. Chiang, A. Paz, S. Hallman, O. Yuan, *et al.*, 2016 Intermittent Stem Cell Cycling Balances Self-Renewal and Senescence of the C. elegans Germ Line. PLoS Genet. 12.

787 Colaiácovo M. P., A. J. MacQueen, E. Martinez-Perez, K. McDonald, A. Adamo, *et al.*, 2003
788 Synaptonemal complex assembly in C. elegans is dispensable for loading strand-exchange
789 proteins but critical for proper completion of recombination. Dev. Cell 5: 463–474.

790 Cruz-García A., A. López-Saavedra, and P. Huertas, 2014 BRCA1 accelerates CtIP-ediated
791 DNA-end resection. Cell Rep. 9: 451–459.

792 Dernburg A. F., K. McDonald, G. Moulder, R. Barstead, and M. Dresser, 1998 Meiotic
793 Recombination in C. elegans Initiates by a Conserved Mechanism and Is Dispensable for
794 Homologous Chromosome Synapsis. Cell 94: 387–389.

795 Doniach T., and J. Hodgkin, 1984 A Sex-Determining Gene, fem-1, Required for Both Male and
796 Hermaphrodite Development in Caenorhabditis elegans. Dev. Biol. 106: 223–235.

797 Gartner A., and J. A. Engebrecht, 2022 DNA repair, recombination, and damage signaling.
798 Genetics 220.

799 Gudgen M., A. Chandrasekaran, T. Frazier, and L. Boyd, 2004 Interactions within the ubiquitin
800 pathway of Caenorhabditis elegans. Biochem. Biophys. Res. Commun. 325: 479–486.

801 Kamp J. A., R. van Schendel, I. W. Dilweg, and M. Tijsterman, 2020 BRCA1-associated
802 structural variations are a consequence of polymerase theta-mediated end-joining. Nat.
803 Commun. 11: 1–10.

804 Keeney S., C. N. Giroux, and N. Kleckner, 1997 Meiosis-Specific DNA Double-Strand Breaks
805 Are Catalyzed by Spo11, a Member of a Widely Conserved Protein Family. Cell 88: 375–
806 384.

807 Kern C. C., S. J. Townsend, A. Salzmann, N. B. Rendell, G. W. Taylor, *et al.*, 2021 C. elegans
808 feed yolk to their young in a form of primitive lactation. Nat. Commun. 12.

809 L'Hernault S. W., 2006 Spermatogenesis. WormBook 1–14.

Li Q., S. Hariri, and J. Engebrecht, 2020 Meiotic double-strand break processing and crossover patterning are regulated in a sex-specific manner by BRCA1-BARD1 in C. elegans. Genetics 216: 359–379.

Libuda D. E., S. Uzawa, B. J. Meyer, and A. M. Villeneuve, 2013 Meiotic chromosome structures constrain and respond to designation of crossover sites. Nature 502: 703–706.

Luo S., W. M. Shaw, J. Ashraf, and C. T. Murphy, 2009 TGF-ß Sma/Mab signaling mutations uncouple reproductive aging from somatic aging. PLoS Genet. 5.

Luo S., G. A. Kleemann, J. M. Ashraf, W. M. Shaw, and C. T. Murphy, 2010 TGF-β and Insulin Signaling Regulate Reproductive Aging via Oocyte and Germline Quality Maintenance. Cell 143: 299–312.

Mack H. I. D., T. Heimbucher, and C. T. Murphy, 2018 The nematode Caenorhabditis elegans as a model for aging research. Drug Discov. Today Dis. Model. 27: 3–13.

Maures T. J., L. N. Booth, B. A. Benayoun, Y. Izrayelit, F. C. Schroeder, *et al.*, 2014 Males shorten the life span of C. elegans hermaphrodites via secreted compounds. Science (80-.). 343: 541–544.

Mccarter J., B. Bartlett, T. Dang, and T. Schedl, 1999 On the Control of Oocyte Meiotic Maturation and Ovulation in Caenorhabditis elegans. Dev. Biol. 205: 111–128.

Moghadam A. R. E., M. T. Moghadam, M. Hemadi, and G. Saki, 2022 Oocyte quality and aging. J. Bras. Reprod. Assist. 26: 105–122.

Pickett C. L., and K. Kornfeld, 2013 Age-related degeneration of the egg-laying system promotes matricidal hatching in Caenorhabditis elegans. Aging Cell 12: 544–553.

Preibisch S., S. Saalfeld, and P. Tomancak, 2009 Globally optimal stitching of tiled 3D microscopic image acquisitions. Bioinforma. Appl. 25: 1463–1465.

833 Raices M., R. Bowman, S. Smolikove, and J. L. Yanowitz, 2021 Aging Negatively Impacts DNA
834 Repair and Bivalent Formation in the C. elegans Germ Line. Front. Cell Dev. Biol. 9.

835 Rosu S., K. A. Zawadzki, E. L. Stamper, D. E. Libuda, and A. L. Reese, 2013 The C. elegans
836 DSB-2 Protein Reveals a Regulatory Network that Controls Competence for Meiotic DSB
837 Formation and Promotes Crossover Assurance. PLoS Genet 9: 1–23.

838 Ruth K. S., F. R. Day, J. Hussain, A. Martínez-Marchal, C. E. Aiken, *et al.*, 2021 Genetic
839 insights into biological mechanisms governing human ovarian ageing. Nature 596: 393–
840 397.

841 Sancho E., M. R. Vila, L. Sanchez-Pulido, J. J. Lozano, R. Paciucci, *et al.*, 1998 Role of UEV-1,
842 an Inactive Variant of the E2 Ubiquitin-Conjugating Enzymes, in In Vitro Differentiation and
843 Cell Cycle Behavior of HT-29-M6 Intestinal Mucosecretory Cells. Mol. Cell. Biol. 18: 576–
844 589.

845 Schedl T., and J. Kimble, 1988 fog-2, a Germ-Line-Specific Sex Determination Gene Required
846 for Hermaphrodite Spermatogenesis in Caenorhabditis elegans. Genetics 119: 46–61.

847 Shi C., and C. T. Murphy, 2014 Mating Induces Shrinking and Death in *Caenorhabditis* Mothers.
848 Science (80-.). 343: 536–540.

849 Shim E. Y., A. K. Walker, and T. Keith Blackwell, 2002 Broad requirement for the mediator
850 subunit RGR-1 for transcription in the Caenorhabditis elegans embryo. J. Biol. Chem. 277:
851 30413–30416.

852 Silva-García C. G., A. Lanjuin, C. Heintz, S. Dutta, N. M. Clark, *et al.*, 2019 Single-copy knock-in
853 loci for defined gene expression in caenorhabditis elegans. G3 Genes, Genomes, Genet.
854 9: 2195–2198.

855 Tang L., T. Machacek, Y. M. Mamnun, A. Penkner, J. Gloggnitzer, *et al.*, 2010 Mutations in
856 Caenorhabditis elegans him-19 Show Meiotic Defects That Worsen with Age. Mol. Biol.

Cell 21: 885–896.

Thompson O., M. Edgley, P. Strasbourger, S. Flibotte, B. Ewing, *et al.*, 2013 The million mutation project: A new approach to genetics in Caenorhabditis elegans. Genome Res. 23: 1749–1762.

Toraason E., V. L. Adler, N. A. Kurhanewicz, A. DiNardo, A. M. Saunders, *et al.*, 2021 Automated and customizable quantitative image analysis of whole Caenorhabditis elegans germlines. Genetics 217.

Vandemark A. P., R. M. Hofmann, C. Tsui, C. M. Pickart, and C. Wolberger, 2001 Molecular Insights into Polyubiquitin Chain Assembly: Crystal Structure of the Mms2/Ubc13 Heterodimer. Cell 105: 711–720.

Wasserzug-Pash P., R. Rothman, E. Reich, L. Zecharyahu, O. Schonberger, *et al.*, 2022 Loss of heterochromatin and retrotransposon silencing as determinants in oocyte aging. Aging Cell 21.

Wickham H., M. Averick, J. Bryan, W. Chang, L. McGowan, *et al.*, 2019 Welcome to the Tidyverse. J. Open Source Softw. 4: 1686.

Wijk S. J. L., and H. T. M. Timmers, 2010 The family of ubiquitin-conjugating enzymes (E2s): deciding between life and death of proteins. FASEB J. 24: 981–993.

Yokoo R., K. A. Zawadzki, K. Nabeshima, M. Drake, S. Arur, *et al.*, 2012 COSA-1 Reveals Robust Homeostasis and Separable Licensing and Reinforcement Steps Governing Meiotic Crossovers. Cell 149: 75–87.